Calcium-Decorated Boron-Doped Graphene for High-Capacity Hydrogen Storage

by

Elham Beheshti Zavareh

B.Sc. (Electrical Engineering), Sharif University of Technology, 2006

A THESIS SUBMITTED IN PARTIAL FULFILLMENT OF

THE REQUIREMENTS FOR THE DEGREE OF

MASTER OF APPLIED SCIENCE

in

The Faculty of Graduate Studies

(Electrical and Computer Engineering)

THE UNIVERSITY OF BRITISH COLUMBIA

(Vancouver)

October, 2009

Abstract

Hydrogen has been viewed as a clean synthetic energy carrier that could replace fossil fuels, especially for transport applications. One bottleneck in developing a hydrogen economy is to find feasible and safe storage materials that can store hydrogen with high gravimetric and volumetric densities at ambient conditions. The U.S. department of energy has set a system target of 6 wt.% hydrogen storage density by 2010 and 9 wt.% by 2015, which has not been met yet.

In this thesis, hydrogen adsorption and storage in calcium-decorated boron-doped graphene is studied by ab initio calculations using density functional theory (DFT). We first consider pure graphene coated with calcium atoms on both sides, supposing that metal atoms are dispersed uniformly on the surface with a calcium coverage of 25%. We find that up to four hydrogen molecules can bind to a Ca atom, which results in a storage capacity of 8.32 wt.%. Then, we address the issue of metal adsorbate clustering. Our calculations show that Ca clustering takes place on pristine graphene because of the small binding energy of Ca to graphene. One way to enhance the metal adsorption strength on the graphene plane is to dope graphene with acceptors such as boron atoms. We show that upon boron doping with a concentration of 12 at.%, the clustering problem could be prevented and the resulting gravimetric capacity is 8.38 wt.% hydrogen.

Contents

List of Tables

List of Figures

Acknowledgments

I am most grateful to my advisor Dr. Peyman Servati for his guidance that he has provided throughout the duration of my M.Sc. It has been a privilege working with him on such an interesting and challenging project.

I owe particular thanks to Dr. Alireza Nojeh for the many productive meetings we had, and whose penetrating questions taught me to question more deeply and helped me to accomplish this work.

Thank you to all my friends and lab mates for their help and encouragement. Special thanks are owed to my beloved parents, who have supported me throughout my years of education with their endless inspiration and guidance. And finally, I would like to thank Soroush for his love and encouragement that pushed me to attempt harder than what I have ever done before.

Dedication

I dedicate this work to my parents.

Statement of Co-Authorship

Chapters 1 and 3 were written by the author. Chapter 2 is a paper ready to be submitted for publication, which is co-authored by myself, Dr. Alireza Nojeh, and Dr. Peyman Servati. I performed the simulation and analysis; I generated and prepared the figures; I wrote the first draft of the paper, and participated in the collaborative effort that led to the final version of the paper.

Chapter 1

Introduction

1.1 Hydrogen fuel cell basics

With an ever increasing energy demand by the world population and limited fossil fuel resources, efficient energy generation and use have become urgent issues. Fuel cells may therefore play an important role in the near future as power sources in the transportation area, for portable electronic items or stationary devices for industrial and domestic use. Fuel cells convert chemical energy directly into electrical energy with high efficiency and low emission of pollutants. Theoretically, the maximum energy efficiency of a fuel cell can be as high as 50-60%, twice as much as that of thermal processes.

The first primitive fuel cell was presented by William Grove in 1839 [1]. He discovered the basic operation principle of fuel cells, which remains unchanged since then even in today's modern fuel cell technology: a fuel cell is an electrochemical device that continuously converts chemical energy into electrical energy (and some heat) as long as the fuel and oxidant are supplied [2].

Different types of fuel cells exist under active development. The proton exchange membrane fuel cell (PEMFC), also known as polymer electrolyte membrane fuel cell, is a type of fuel cell which typically operates on pure hydrogen fuel. PEMFCs are considered to have high energy density and quick start up time. Therefore, PEMFCs are believed to be the best type of fuel cell to eventually replace gasoline and diesel internal combustion engines.

1.1.1 How a hydrogen fuel cell works

A whole family of fuel cells exists with different designs, but all these fuel cells work based on the same basic principle. A schematic PEMFC and the way it operates is illustrated in Figure 1.1. A fuel cell converts chemical energy to electrical energy and produces electricity from fuel and oxidant. The reactant fuel (i.e. hydrogen) is channeled through the anode side of the cell and separated to electrons and protons in the presence of a catalyst which is typically a platinum alloy. The oxidant (usually oxygen from air) is channeled through the cathode side and is reduced to oxide ions. In PEMFCs, fuel and oxidant react in the presence of an electrolyte (a solid polymer membrane) which is electronically insulating but conducts the positively charged ions. Therefore, the protons from the anode side are transported through the electrolyte to combine with the oxide ions at the other side and form water as a waste product. Eventually, the negatively charged electrons (which cannot pass through the electrolyte) must travel along an external circuit to the other side and generate electricity.

Typically, the power generated by a fuel cell is barely enough for most applications. Therefore, to produce the desired amount of electricity, individual fuel cells are combined in series or parallel circuits and form a *fuel cell stack*. A fuel cell stack may be comprised of a few or a huge number of single cells, which makes it ideal for a wide variety of applications from laptop computers (50-100 Watts) to central power generations (1-200 MW or more) [3].

1.1.2 Hydrogen as a future energy carrier

Hydrogen is the lightest element in the periodic table and its electron (valence electron) is accompanied by only one proton; thus, the hydrogen molecule has the highest energy gain per electron and energy-to-mass ratio of any chemical. The chemical energy per mass of hydrogen is 142 $MJkg^{-1}$, which is approximately three times more
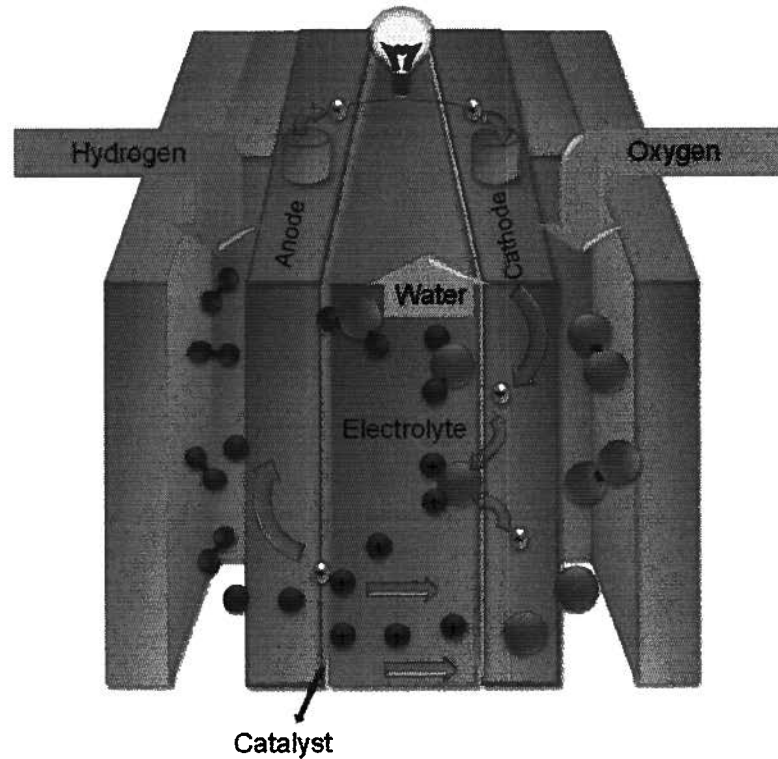
Figure 1.1: Schematic model of a hydrogen fuel cell. At the anode side, hydrogen fuel is channeled through the cell. Then, a catalyst causes the hydrogen to split into hydrogen ions (H^+) and electrons. At the next step, the electrolyte allows the hydrogen ions to pass between the anode and the cathode. Consequently, electrons (which cannot pass through the electrolyte) pass through an external circuit to the cathode. At the cathode, channeled oxygen reacts with electrons and hydrogen ions to form water as a waste product, which flows out of the cell.

than that of other fuels (e.g. the equivalent value for liquid hydrocarbons is 47 $MJkg^{-1}$) [4]. Hydrogen is a clean synthetic fuel: it is not comprised of carbon; it is non-toxic; and its waste product by either thermal or electrochemical combustion is only water vapor.

Hydrogen is the most abundant element on Earth, but it can barely be present as molecular hydrogen gas H_2 (less than 1%); it combines readily with other elements such as oxygen or carbon. Thus, the majority of hydrogen is in H_2O form and some is in the form of hydrocarbons. In other words, the main source of hydrogen is water, which is essentially an unlimited resource and its amount is easily more than enough to sustain a hydrogen economy for widespread use. The clean way to extract hydrogen from water is to use renewable energy sources such as wind or solar power (photovoltaic cells) or hydro-electric power. Hydrocarbons, the other source of hydrogen, such as methanol, ethanol, and natural gas can yield hydrogen by a fuel reforming process. Moreover, hydrogen can be extracted from biomass technologies.

The main problem with hydrogen as a fuel is that although its energy content by weight is very high, it has a very low energy content by volume (8 MJ/liter for liquid hydrogen versus 32 MJ/liter for gasoline) [5]; hydrogen is a gas at room temperature and it takes an extremely large amount of space. Thus, to have on-board energy storage for mobile applications, hydrogen gas must be compressed in some way.

Using today's technology, a modern, safe car weighs 1.2-1.5 tons. This car is optimized to travel a range of 500 km burning 30-35 liters of petrol in a combustion engine. A hydrogen fuel cell electric motor system would need about 5 kg of hydrogen to travel the same range (in case of a car fitted with a hydrogen combustion engine, 10 kg or more of hydrogen is needed). Here is the main problem: at room temperature and atmospheric pressure, 5 kg of hydrogen occupies about 56,000 liters, which corresponds to a balloon of 4.8 m diameter. Consequently, using hydrogen in its gaseous form is not practical for a vehicle and it is essential to find a method to squeeze the hydrogen volume down by at least 1000 times [6].

1.2 Hydrogen storage

One of the main challenges in developing fuel cell technology for mobile applications is to find a compact, light-weight hydrogen storage system. A desirable hydrogen storage system needs to be capable of delivering hydrogen gas to a fuel cell at approximately room temperature and at a pressure not much greater than atmospheric pressure (1 bar). In 2002, the U.S. Department of Energy (DOE) set system targets for the hydrogen content of storage media: the DOE target is 6% by mass (or 6 wt.%, i.e. at least 6% of the storage system weight is usable H_2 weight) by 2010, and then 9 wt.% by 2015. So far, the targets have not been met while intensive research has been conducted in this area.

Hydrogen can be stored in different forms. The goal is to pack hydrogen gas as densely as possible, i.e. to reach the highest volumetric density by using as little additional material as possible. Besides conventional storage methods, i.e. high pressure gas tanks and liquid hydrogen, hydrogen can be reversibly absorbed or adsorbed by certain solid materials, greatly reducing its volume. Materials-based hydrogen storage includes physisorption of hydrogen on solids with a high specific surface area and hydrogen intercalation in metals and complex hydrides [1].

1.2.1 Compressed gas and liquid hydrogen tanks

Hydrogen can be stored at high pressure or in liquefied form to reduce the volume. The energy density of hydrogen gas can be improved by compressing hydrogen and storing it at higher pressures. Classical high-pressure tanks made of steel can take up to 300 bar (30 MPa) and be filled up to 200 bar. However this is still not a practical solution for on-board hydrogen storage; to store 5 kg of hydrogen it requires a volume of 280 liters. The pressure of the tank can be as high as 600 bar by new high-pressure tanks, which are made of carbon-fiber-reinforced materials. To prevent

---

[1]A *hydride* is a chemical compound in which hydrogen is combined with another element.

the reaction between hydrogen and polymer, another approach is to use hydrogen-inert aluminum tanks, which are strengthened with external carbon-fiber coating. These novel containers can store hydrogen up to 4 wt.% [4].

Using high pressure tanks has significant disadvantages: hydrogen cannot be used in such a high pressure for the fuel cell and it is thus essential to have additional pressure control. Furthermore, both compressing hydrogen and storing it at high pressure are highly dangerous and safety issues would become a serious concern.

Condensing into liquid hydrogen results in hydrogen in an extremely energy-dense form. But the condensation temperature of hydrogen at atmospheric pressure (1 bar) is -250 $^\circ C$ [6]. Therefore, the energy requirement for hydrogen liquefaction is high; it results in a loss of about 30% of the generated energy for liquefaction [5]. Additionally, the required cryogenic techniques are not feasible for ordinary fuel stations.

1.2.2 Materials-based hydrogen storage

Hydrogen molecules or atoms bound with other elements in potential storage materials make it possible to have a storage medium with larger capacities (i.e. larger quantities of hydrogen in smaller volumes) at low pressure and near room temperature. There are two main classes of hydrogen storage in materials, corresponding to two different sorption mechanisms: *physisorption* and *chemisorption*. Whereas in physisorption hydrogen molecules are weakly adsorbed by the material and stored on its surface, in chemisorption hydrogen molecules are dissociated into hydrogen atoms and absorbed into the bulk material through a chemical reaction.

In material-based hydrogen storage, hydrogen needs to be released by heat and lowering the pressure. Consequently, an efficient hydrogen storage medium has to be reversible, i.e. the uptake and release of hydrogen need to take place at the pressure and temperature range attractive for mobile storage (1-10 bar, 0-100 $^\circ C$) [4].

Moreover, having a high gravimetric capacity (wt.%) of hydrogen uptake is the most critical challenge for different media.

Hydrogen storage by metal hydrides

Certain metals and alloys (and also other chemical compounds) are capable of reacting with hydrogen (chemisorption) and forming hydrides. This reaction results in a fast and reversible absorption of a large amount of hydrogen molecules at practically accessible temperatures. Figure 1.2 shows the steps of hydride formation: H_2 is dissociated at the surface of the metal; then, hydrogen atoms adopt random locations in the host metal lattice; finally, hydrogen atoms make metallic, covalent, or ionic bonds with the material in a regular arrangement. The metal lattice expands during this process and mostly loses its high symmetry.

Many different hydrides of either elemental metals (e.g. Pd and Mg) or compounds have been studied as appropriate hydrogen storage materials. For instance, alloys derived from $LaNi_5$ show some very promising properties forming $LaNi_5H_6$. Hydrogen-volume density in most of these materials is far above that of liquefied hydrogen. However, because the host materials are large elements the amount of hydrogen stored in these materials has not yet exceeded 4 wt.%; the proportion of hydrogen in $LaNi_5H_6$ is too low (about 1.3 wt.%) and it is not practical for mobile applications.
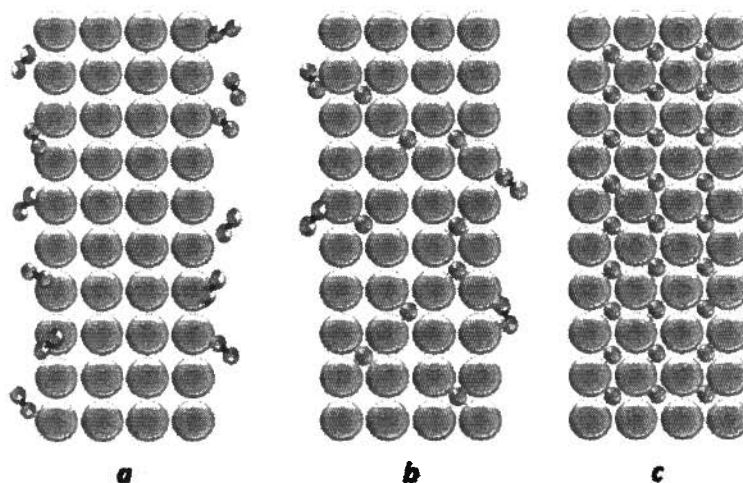
Figure 1.2: Schematic model of hydrogen storage by metal hydrides. **(a)** First, the hydrogen molecules react with the surface of the metal and dissociate into separate H atoms. **(b)** Then, single hydrogen atoms adopt random locations in the metal lattice. **(c)** Finally, the hydrogen atoms form a regular arrangement in the lattice and make metallic, covalent, or ionic bonds with the metal.

Many promising new ideas are being studied with the goal of increasing the hydrogen mass density in hydrides. New families of alloys are being explored based on some metals such as vanadium and titanium [4]. One approach is to achieve higher mass density by using light metal elements such as calcium and magnesium. But the reaction of forming hydrides with these lighter elements is extremely low and is reversible only at very high temperatures.

Hydrogen adsorption on solids with large surface area

Hydrogen can be adsorbed *on the surface of solids* via weak van der Waals interaction (physisorption). In the physisorption scheme, light porous materials with very large

surface area are potential candidates for hydrogen storage applications (Figure 1.3). In this scheme, it is desirable to make use of light elements with porous structures from the first row of the periodic table. Among these elements, there has been considerable interest in the possible use of carbon as the hydrogen storage material.
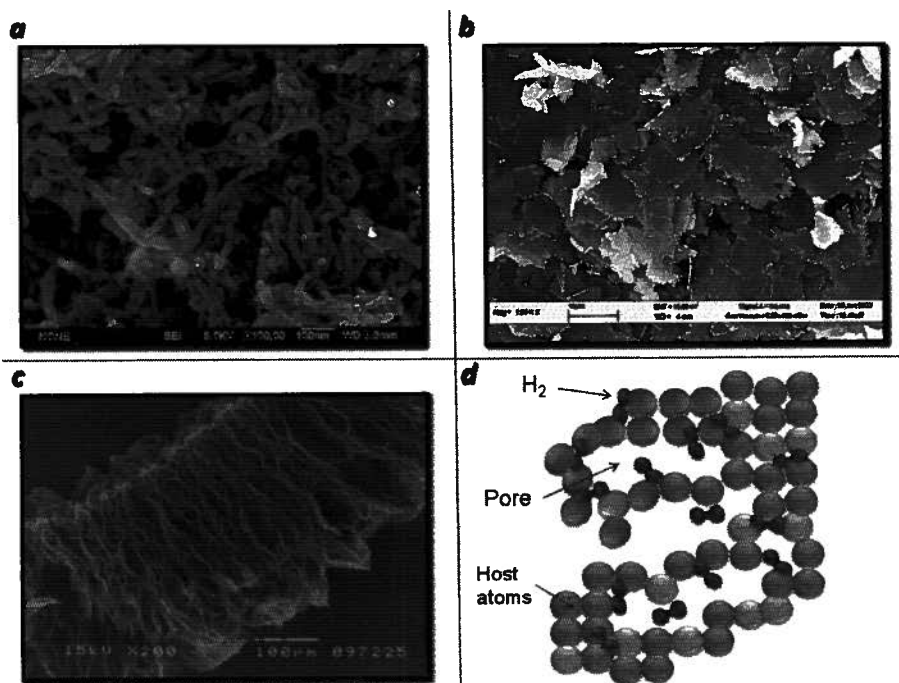
Figure 1.3: Porous carbonaceous materials with high surface area. SEM images of the porous structure of (**a**) activated carbon nanotube (CNT). Reprinted with permission from [7]. Copyright @ 2002 Elsevier Science Ltd. (**b**) foliated graphite sheets prepared upon 10 h of ultrasonic irradiation. Reprinted with permission from [8]. Copyright @ 2004 Elsevier Science Ltd. (**c**) exfoliated graphite sheet. Reprinted with permission from [9]. Copyright @ 2001 Elsevier Science Ltd. (**d**) Schematic model of hydrogen storage by materials with high porosity. In this scheme, hydrogen gas molecules accumulate at the surface of the material, but they do not react chemically with the host material.

Recent developments of carbonaceous material synthesis have resulted in several new forms of carbon nanostructures such as fullerenes, carbon nanotubes, carbon nanofibers, and graphene sheets. There are hypotheses that these carbon nanomaterials may have extraordinarily high hydrogen storage capacities due to their high surface area and porous structure [10]. In the next section, we will discuss different carbon nanostructures as the potential hydrogen storage medium.

1.3 Hydrogen storage in carbon nanostructures

There are several different types of carbon materials with potential for hydrogen storage. Early work in this area focused on the hydrogen adsorption properties of activated carbon. Activated carbon (AC) is a synthetic carbon containing very small graphite crystallites and amorphous carbon which has been processed to make it extremely porous. Thus, activated carbon could have a very large specific surface area [2] of up to 3000 m^2g^{-1} ,with pore diameters of less than 1 nm [11]. The hydrogen storage properties of activated carbons have been extensively studied. However, AC is not an efficient hydrogen storage medium as only a small fraction of the pores are small enough to interact strongly with hydrogen molecules at ambient conditions. More than 50% of the total pore volume of AC are macropores which are not useful for ambient temperature hydrogen storage [12]. Thus conventional carbon adsorbents exhibit poor hydrogen uptakes, which has motivated the development of novel carbon nanomaterials with high surface area and appropriate pore size that are more specifically designed for hydrogen storage.

Graphite nanofibers (GNF) and multi-walled and single-walled carbon nanotubes (MWNT and SWNT, respectively) are examples of engineered carbon materials that have recently been investigated for hydrogen storage. For the first time, in 1997 Dillon et al. [13] reported excellent hydrogen storage properties of soots containing SWNTs. The hydrogen storage capacity was estimated to be about 5 to 10 wt.% at

---

[2] *Specific surface area* is a property of solids measured as the total surface area per unit of mass.

133 K and 40 kPa. Chambers et al. [14] (1998) reported their findings on various carbon nanostructures. They observed that at 11 MPa and room temperature, GNFs with herringbone structure could uptake hydrogen up to 67 wt.%. This extraordinarily high value caused an avalanche of research on hydrogen storage in CNTs. However, until today, nobody has been able to reproduce their results [15]. In any case, all the reports with promising results for hydrogen uptake in GNF and CNT point to the necessity of high pressure or subambient temperature (or both).

In contrast to these promising reports, Ritschel et al. [16] (2002) found a limited hydrogen uptake (less than 1 wt%) in different forms of carbon nanostructures (SWNT, MWNT and GNF). In agreement with their results, Hirscher et al. [17] found a low hydrogen storage capacity in all forms of carbon nanostructures. They studied hydrogen storage on SWNT, MWNT, and GNF structures and found a small reversible hydrogen uptake only for SWNTs. In their report in 2005 [18], they observed that different carbonaceous materials with different structures show similar adsorption properties. Moreover, a linear relation between hydrogen uptake and specific surface area is obtained for all samples, which is independent of the nature and structure of the carbon material. The best material with a specific surface area of 2560 m^2g^{-1} shows a storage capacity of 4.5 wt% at 77 K.

As far as the specific surface area is concerned, a single layer of graphene may be superior to other carbon nanostructures because both of its sides can be readily utilized for hydrogen adsorption.

Graphene is a single planar sheet of sp^2 bonded carbon atoms packed into a two-dimensional (2D) honeycomb lattice, which is identical to one isolated layer of the graphite structure. Graphene can be wrapped up into 0D fullerenes, rolled into 1D nanotubes or stacked into 3D graphite (Figure 1.4). For more than 70 years, graphene has been studied extensively in theory for describing different carbon materials. However, an isolated graphene layer was assumed to be unstable, leading to the formation of stable curved structures such as carbon soot, fullerenes and nanotubes. Very recently (in 2004), Novoselov et al. [19] found a way to isolate graphene by peeling it

off from graphite with Scotch tape. Using the density of graphite ($\rho = 2267\ kgm^{-3}$) and assuming that all the atoms are in one single plane the maximum specific surface area of graphene is S_1=1315 m^2g^{-1}, or in case of considering both sides of graphene, S_2=2630 m^2g^{-1}. Therefore, graphene has a high specific surface area compared to the outer surface area of nanotubes [15].
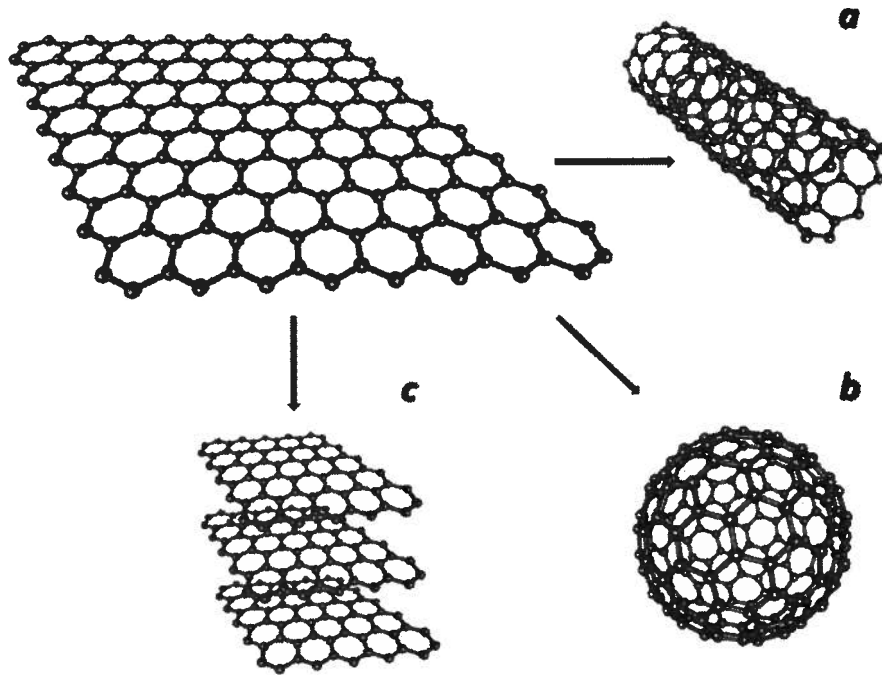
Figure 1.4: Graphene as a 2D building material for carbon materials of all other dimensionalities. It can be (a) rolled into 1D carbon nanotubes, (b) wrapped up into 0D buckballs, or (c) stacked into 3D graphite.

1.3.1 The optimum conditions for adsorptive storage on carbon nanostructures

Storage materials should be able to reversibly adsorb/desorb hydrogen molecules in a desirable range of temperature and pressure. The affinity of hydrogen to the adsorbent material should be strong enough to store a large amount of hydrogen gas at the charging pressure (about 30 bar), but at the same time weak enough to release most of the hydrogen at the discharge pressure (about 1.5 bar). Recently, Bhatia et al. [20] have examined the optimum thermodynamic conditions for hydrogen storage. Based on their studies, the optimal adsorption energy for hydrogen should be in the range of 0.2-0.4 eV/H_2 at room temperature. This range of binding energy is the intermediate between physisorbed and chemisorbed states.

For carbon in any form, binding energies are too low for storing hydrogen at ambient temperature. Both experimental and theoretical studies indicate that the interaction between hydrogen molecules and the carbon nanostructure is due to physisorption. Brown et al. [21] showed experimentally that hydrogen physisorbs on the curved exterior surface of SWNTs with the binding energy of 6-40 meV at 25 K. Also, the hydrogen binding energy is calculated to be in the range of 30-60 meV on SWNTs and graphene sheets by theoretical studies [22, 23, 24, 25]. Therefore, it is essential to find a way to enhance the binding energy on the carbon nanostructure surface. In recent years, many studies have been conducted on functionalized carbon nanostructures such as metal-coated structures.

1.3.2 Metal-coated carbon nanostructures

For hydrogen storage, pristine carbon nanostructures are chemically too inert to make strong enough binding with hydrogen molecules at room temperature. One approach to increase their chemical activity is using metal decorated structures by adding alkali metals [3] or transition metals (TMs) as the coating material. In 1999, Chen et

---

[3]Alkali metals constitute the first group of periodic table.

al. [26] reported that alkali-metal-doped (lithium- or potassium-doped) carbon nanotubes are capable of high hydrogen uptake. However, the binding sites for these metals are still too weak. In recent years, light transition metals such as titanium and scandium have attracted much attention as the coating material. It has been shown theoretically that TM-coated fullerenes and nanotubes can store up to 8 wt.% hydrogen with a binding energy of 0.3 eV/H_2 [27, 28]. In these studies, TM atoms were assumed to be uniformly distributed on the surface. However, TM atoms tend to form clusters on the surface of carbon nanostructures and it is thus very difficult to achieve uniformly coated monolayers of TM atoms experimentally [29]. Consequently, the hydrogen storage capacity drops dramatically. Moreover, TM-coated systems are highly reactive, which leads to the dissociation of the first adsorbed hydrogen molecule.

In 2008, Yoon et al. [30] found using theoretical calculations that the clustering can be prevented in Ca-coated C_{60} systems. Calcium is an alkaline-earth metal, between the too weak alkali and the too reactive transition metals, which has empty d orbitals. The strong binding of Ca results from the charge transfer mechanism involving its empty $3d$ orbitals. The Ca atom donates part of its charge to C atoms, which gives rise to an electric field between the Ca atom and the substrate. Due to this field, part of the donated charge is back donated to the empty $3d$ orbitals of the Ca atom. This charge redistribution mechanism enhances the polarization of the H_2 molecules and thus the binding energy of hydrogen is increased.

1.4 Research objectives

The objective of this research is to find the hydrogen storage capacity of calcium-decorated graphene using first-principles calculations. In this work, we first address critical questions in determining the storage capacity of a calcium-decorated structure: (i) What is the effective coverage of calcium atoms adsorbed on graphene that can be attained for single-sided or double-sided adsorption? (ii) How many hydro-

gen molecules can be adsorbed on each calcium atom? and (iii) What is the average binding energy of hydrogen?

Next, we address the important issue of calcium stability on the graphene plane. In contrast to previous studies [31], we show that for dense coverage of calcium on graphene, calcium aggregation takes place, which decreases the storage capacity of the system. The next question that we address is how to prevent calcium clustering on graphene.

Yang et al. have recently (in February 2009) investigated the stability of calcium adsorbates on carbon nanotubes and defective graphene. In their theoretical studies, they considered graphene with pentagonal and octagonal defects. They found that calcium is stable on defective graphene. Later (in September 2009), Lee et al. [32] investigated calcium-decorated carbon nanotubes for hydrogen storage. They suggested that upon boron doping the calcium clustering problem could be prevented. They also showed that individual Ca-decorated B-doped carbon nanotubes with a concentration of $\sim$ 6 at.% B doping can reach a gravimetric capacity of $\sim$ 5 wt.% hydrogen. Here, we consider boron-doped graphene with different concentrations of boron atoms and study the optimal doping concentration for a stable decoration of Ca on graphene.

1.5 Methodology: first-principles calculations

Our first-principles calculations were mainly conducted at the density functional theory (DFT) level. The DFT calculations were carried out by using SIESTA [33] and Gaussian 03 [34] simulation packages. The details and parameters used in calculations are mentioned in chapter 2.

SIESTA is based on DFT, making available both local density and generalized gradient functionals. In SIESTA, core electrons are replaced by norm-conserving pseudopotentials, which are factorized in the Kleinman-Bylander nonlocal form [35].

The pseudopotentials were constructed using the Troullier and Martins parametrization [36] to describe the ion-electron interaction. The one particle problem is then solved using a linear combination of atomic orbitals (LCAO) basis set. The basis functions are flexible both in the radial shape of the orbitals and the size of the basis, but they go to zero beyond a certain radius. We have selected a double-ξ singly polarized (DZP) basis set for all the species and also added diffuse functions for C atoms to produce the band structure of graphene more accurately. Forces on the atoms and the stress tensor are obtained from the Hellmann-Feynman theorem and are used for structure relaxations. Systems are treated in a supercell scheme, which uses three lattice vectors to describe the periodicity. The exchange and correlation potential was treated using both the local density (LDA) and generalized gradient (GGA) approximation functionals. The Ceperely-Alder [36] and Perdew-Burke-Ernzerhof [37] parametrizations were used for LDA and GGA functionals, respectively.

First, the optimized atomic positions of different periodic structures were obtained by relaxing them using the conjugate gradient algorithm. Then we calculated the binding energies of metal atoms and hydrogen molecules as follows:

$$E_{binding} = E_{AB} - (E_A + E_B) \tag{1.1}$$

In equation 1.1, all energies were calculated for the corresponding optimized structures. Hydrogen adsorption on the substrates in this study mainly originates from van der Waals (vdW) interactions. The weak vdW interaction is usually evaluated by using the second-order perturbation theory. Therefore, we also benchmarked our results with second-order *Moller–Plesset* perturbation theory (MP2) [38] and checked the reliability of our DFT calculations. We have performed DFT and MP2 calculations using Gaussian 03 [34] simulation package for a molecular model of coronene [4].

For our calculations within Gaussian 03, We used both a large basis set and the intensive convergence criterion (10^{-4} eV for total energy) to obtain accurate results.

---

[4] *Coronene* $(C_{24}H_{12})$ is a hydrocarbon consisting of six benzene rings passivated with H atoms

The structural optimizations and binding energy calculations were performed using double-zeta polarized 6-31G(d,p) and triple-zeta polarized 6-311G(d,p) basis sets, respectively. In our DFT calculations in Gaussian, GGA was described by the PBE functional. Also, LDA is described by the Slater exchange plus Vosko-Wilk-Nusair correlation (SVWN5) [39], which fits the Ceperely-Alder solution to that of the uniform electron gas [40].

Bibliography

[1] Grove, W. R. *Phil. Mag.* **1839**, *14*, 127–130.

[2] *Fuel Cell Technology Handbook*; Hoogers, G., Ed.; CRC Press LLC: Corporate Blvd., Boca Raton, Florida 33431, 2002.

[3] Steele, B. C. H.; Heinzel, A. *Nature (London)* **2001**, *414*, 345–352.

[4] Schlapbach, L.; Züttel, A. *Nature (London)* **2001**, *414*, 353–358.

[5] Cleveland, C. J. *Hydrogen Storage, The Encyclopedia of Earth*, 2008.

[6] Schlapbach, L. *Nature* **2009**, *460*, 809–811.

[7] Jiang, Q.; Qu, M.; Zhou, G.; Zhang, B.; Yu, Z. *Matter. Lett.* **2002**, *57*, 988–991.

[8] Chen, G.; Weng, W.; Wu, D.; Wu, C.; Lu, J.; Wang, P.; Chen, X. *Carbon* **2004**, *42*, 753–759.

[9] Inagaki, M.; Suwa, T. *Carbon* **2001**, *39*, 915–920.

[10] *Perspectives of Fullerene Nanotechnology*; Osawa, E., Ed.; Kluwer Academic Publishers: Dordrecht, The Netherlands, 2002; pp 327–329.

[11] Ströbel, R.; Garche, J.; Moseley, P. T.; Jörissen, L.; Wolf, G. *J Power Sources* **2006**, *159*, 781–801.

[12] Dillon, A. C.; Heben, M. J. *Appl. Phys. A* **2001**, *72*, 133–142.

[13] Dillon, A. C.; Jones, K. M.; Bekkedahl, T. A.; Kiang, C. H.; Bethune, D. S.; Heben, M. J. *Nature* **1997**, *386*, 377–379.

[14] Chambers, A.; Park, C.; Baker, R. T. K.; Rodriguez, N. M. *J. Phys. Chem. B* **1998**, *102*, 4253–4256.

[15] Züttel, A.; Sudan, P.; Mauron, P.; Kiyobayashi, T.; Emmenegger, C.; Schlapbach, L. *Int. J. Hydrogen Energy* **2002**, *27*, 203–212.

[16] Ritschel, M.; Uhlemann, M.; Gutfleisch, O.; Leonhardt, A.; Graff, A.; Täschner, C.; Fink, J. *Appl. Phys. Lett.* **2002**, *80*, 2985–2987.

[17] Hirscher, M.; Becher, M.; Haluska, M.; Quintel, A.; Skakalova, V.; Choi, Y. M.; Dettlaff-Weglikowska, U.; Roth, S.; Stepanek, I.; Bernier, P.; Leonhardt, A.; Fink, J. *J Alloys and Compd* **2002**, *330-332*, 654–658.

[18] Panella, B.; Hirscher, M.; Roth, S. *Carbon* **2005**, *43*, 2209–2214.

[19] Novoselov, K. S.; Geim, A. K.; Morozov, S. V.; Jiang, D.; Zhang, Y.; Dubonos, S. V.; Grigorieva, I. V.; Firsov, A. A. *Science* **2004**, *306*, 666–669.

[20] Bhatia, S. K.; Myers, A. L. *Langmuir* **2006**, *22*, 1688–1700.

[21] Brown, C.; Yildirim, T.; Neumann, D.; Heben, M.; Dillon, T. G. A.; Alleman, J.; Fischer, J. *Chem. Phys. Lett.* **2000**, *329*, 311–316.

[22] Dag, S.; Ozturk, Y.; Ciraci, S.; Yildirim, T. *Phys. Rev. B* **2005**, *72*, 155404.

[23] Han, S. S.; Lee, H. M. *Carbon* **2004**, *42*, 2169–2177.

[24] Arellano, J. S.; Molina, L. M.; Rubio, A.; López, M. J.; Alonso, J. A. *J Chem. Phys.* **2002**, *117*, 2281.

[25] Arellano, J. S.; Molina, L. M.; Rubio, A.; Alonso, J. A. *J Chem. Phys.* **2000**, *112*, 8114.

[26] Chen, P.; Wu, X.; Lin, J.; Tan, K. L. *Science* **1999**, *285*, 91–93.

19

[27] Zhao, Y.; Kim, Y.; Dillon, A. C.; Heben, M. J.; Zhang, S. B. *Phys. Rev. Lett.* **2005**, *94*, 155504.

[28] Yildirim, T.; Ciraci, S. *Phys. Rev. Lett.* **2005**, *94*, 175501.

[29] Zhang, Y.; Franklin, N. W.; Chen, R. J.; Dai, H. *Chem. Phys. Lett.* **2000**, *331*, 35–41.

[30] Yoon, M.; Yang, S.; Hicke, C.; Wang, E.; Geohegan, D.; Zhang, Z. *Phys. Rev. Lett.* **2008**, *100*, 206806.

[31] Ataca, C.; Aktürk, E.; Ciraci, S. *Phys. Rev. B* **2009**, *79*, 041406.

[32] Lee, H.; Ihm, J.; Cohen, M. L.; Louie, S. G. *Phys. Rev. B* **2009**, *80*, 115412.

[33] Soler, J. M.; Artacho, E.; Gale, J. D.; García, A.; Junquera, J.; Ordejón, P.; Sánchez-Portal, D. *J. Phys.: Condens. Matter* **2002**, *14*, 2745–2779.

[34] Frisch, M. J. et al. *Gaussian 03, Revision C.02*, Gaussian, Inc., Wallingford, CT, 2004.

[35] Kleinman, L.; Bylander, D. M. *Phys. Rev. Lett.* **1982**, *48*, 1425–1428.

[36] Troullier, N.; Martins, J. L. *Phys. Rev. B* **1991**, *43*, 1993–2006.

[37] Perdew, J. P.; Burke, K.; Ernzerhof, M. *Phys. Rev. Lett.* **1996**, *77*, 3865–3868.

[38] Moller, C.; Plesset, M. S. *Phys. Rev.* **1934**, *46*, 618–622.

[39] Vosko, S. H.; Wilk, L.; Nusair, M. *Can. J. Phys.* **1980**, *58*, 1200.

[40] Ceperley, D. M.; Alder, B. J. *Phys. Rev. Lett.* **1980**, *45*, 566–569.

Chapter 2

Calcium-Decorated Boron-Doped Graphene for High-Capacity Hydrogen Storage: A First-Principles Study

2.1 Introduction

Hydrogen has been viewed as a clean energy carrier that could replace fossil fuels, particularly for transport applications such as hydrogen fuel cell vehicles.[1] One of the main challenges in developing hydrogen fuel cell technology for mobile applications is to find a compact, safe and affordable storage system. A desirable system would be capable of storing hydrogen with high gravimetric and volumetric densities at near room temperature and ambient pressure. The U.S. Department of Energy has set a system target of 6 wt.% hydrogen storage density by 2010 and 9 wt.% by 2015. Furthermore, hydrogen recycling (hydrogen adsorption and desorption) should be performed reversibly in a feasible range of temperature and pressure, which requires the optimal hydrogen adsorption energy of 0.2-0.4 eV/H_2 [2, 3]. This range of energy is intermediate between the physisorbed and chemisorbed states. Many different

---

A version of this chapter will be submitted for publication. Beheshti-Zavareh, E., Nojeh, A., and Servati, P. Calcium-Decorated Boron-Doped Graphene for High-Capacity Hydrogen Storage: A First-Principles Study.

techniques such as using metal hydrides, liquefied hydrogen or high pressure tanks have been investigated for hydrogen storage, nevertheless, these techniques have several drawbacks such as low capacity, non-reversibility or safety problems. Recently, carbon nanomaterials with high specific surface area have been widely studied for hydrogen storage [4, 5, 6]. However, for carbon in any form, the interaction with H_2 is through weak van der Waals forces [7, 8, 9]. Therefore, binding energies are too low for storing hydrogen at ambient conditions and it is essential to find a way to enhance the binding energy on the carbon nanostructure surface.

In recent years, many studies have been devoted to functionalizing the surface of carbon nanostructures with transition metals (TMs) [10, 11, 12, 13] to provide possible systems for hydrogen storage applications. A TM atom interacts with the carbon substrate and hydrogen molecules through Dewar [14] and Kubas [15] interactions, respectively. The combination of these two interactions, in which the TM's $3d$ orbitals are involved, enhances the binding energy of hydrogen to TM atoms. Yildirim et al. [11] and Zhao et al. [12] showed that TM-coated fullerenes and nanotubes can store up to 8 wt.% hydrogen with the average binding energy of 0.3 eV/H_2. In these studies, TM atoms were assumed to be uniformly distributed on the surface. However, because of their large cohesive energy, TM atoms tend to cluster on the surface of carbon nanostructures and it is thus difficult to achieve uniformly-coated monolayers of TM atoms experimentally. Consequently, the achievable hydrogen storage capacity is low [10, 16, 17]. Moreover, TM-coated systems are highly reactive, which leads to the dissociation of the first adsorbed hydrogen molecule [12].

One possible way to have stable adsorbates without clustering tendency is to use metals with relatively smaller cohesive energy such as alkali [18, 19] (AM) or alkaline earth metals (AEM). Whereas alkali atoms can be coated uniformly, the binding sites for these systems are too weak and the nature of the bonding remains physisorption [20]. Calcium, the first AEM atom with empty $3d$ orbitals, has recently emerged as a superior element to improve the storage capacity in carbon nanomaterials [21, 22, 23, 24]. Yoon et al. [21] have suggested Ca-coated C_{60} fullerenes ($Ca_{32}C_{60}$) for high capacity hydrogen storage (2.7 H_2 per Ca, which results in 8.4 wt.% capac-

ity). Using density functional theory, they have shown that among AEM atoms, Be and Mg cannot be stabilized on C_{60} whereas Ca can decorate these materials through the electron donation/back-donation mechanism, which involves Ca's empty *3d* orbitals [21]. This mechanism stabilizes the chemical interaction between Ca and the carbon nanomaterial. Moreover, Ca could bind with hydrogen more strongly than the AM atoms or earlier AEM atoms (i.e. Be and Mg) due to the hybridization of its 3d orbitals with hydrogen's σ orbitals. However, structural stability is still an issue for Ca-coated carbon nanomaterials. In fact, Ca has less tendency of clustering compared with TM atoms due to its smaller cohesive energy (1.8 eV) [25]. Nevertheless, Ca atoms aggregation takes place on graphitic materials as Ca's binding energy on the carbon absorbent is still lower than that of Ca bulk structure [23, 26].

In this letter, we investigate hydrogen adsorption on calcium-decorated boron-doped graphene using first-principles calculations. Graphene, a monolayer of graphite, is a precursor to C_{60} and carbon nanotubes and has been recently synthesized, showing unusual electronic and magnetic properties [27]. Using both sides of the plane, graphene has a high specific surface area (S=2630 $m^2 g^{-1}$), much higher than the outer surface area of nanotubes [28]. Assuming individually dispersed Ca atoms on graphene, we have shown that Ca atoms bonding to both sides of a graphene plane can uptake 4 hydrogen molecules each, which results in a storage capacity of 8.32 wt.% for a dense coverage of Ca on a (2 × 2) cell.

To prevent metal aggregation and achieve a high-capacity storage material, it is essential to enhance the adsorption energy of Ca on graphene by introducing defects or doping. Yang et al. [25] investigated the effect of surface configuration on the stability of Ca adsorbates and found that Ca atoms are stable on graphene with pentagonal or octagonal defects. Here, instead of considering defective graphene, we explore boron-doped graphene as a solution for the clustering problem. The empty p_z orbital of boron acts as a strong charge acceptor and consequently the strength of Ca adsorption on graphene could be enhanced. Boron could be easily incorporated in the hexagonal structure of graphene without changing the structure drastically and boron-doped graphene has been synthesized experimentally [29, 30].

2.2 Computational details

Our ab initio calculations were performed using density functional theory (DFT) and the SIESTA software package [31]. The self-consistent DFT code is based on a numerical atomic basis set and the core electrons are replaced by norm-conserving pseudopotentials in their fully nonlocal form [32]. The pseudopotentials were constructed using the Troullier and Martins parametrization [33] to describe the ion-electron interaction. The exchange and correlation potential was treated using the local density approximation (LDA) with Perdew-Zunger parametrization [34]. Furthermore, we compared the LDA results with those of the generalized gradient approximation (GGA) with the Perdew-Burke-Ernzerhof [35] (PBE) functional. The use of any of these approximations with DFT calculations to describe van der Waals contributions is still controversial. However, previous studies showed that GGA underestimates the relatively weak binding energies whereas LDA overestimates the interaction [36]. To evaluate the reliability of our LDA and GGA calculations, we also performed second-order Moller–Plesset (MP2) perturbation theory calculations [37] as will be detailed later. We observed that LDA gives results very close to those of MP2 for both energies and structures.

The pseudopotential for Ca is constructed using a partial core correction [38], which accounts for the nonlinear interaction of the core and valence densities in the calculations. We selected a double-ξ singly polarized (DZP) basis set and to obtain a well balanced basis, we used atomic orbitals with the fixed common energy shift of 50 meV for all the species. We also added a diffuse $3s$ orbital for C to produce the band structure of graphene with the description of the electronic spectrum above the Fermi level the same as in plane wave methods [39]. Moreover, for Ca, the $3p$ semicore state was included together with the valence states.

The charge density was projected onto a real-space grid with an equivalent kinetic energy cutoff of 200 Ry, which provides well-converged results equivalent to plane wave calculations. Adsorption of the calcium atoms and hydrogen molecules is treated within the supercell geometry with lattice parameters $a_{SC}=b_{SC}=4.92$ Å and $c_{SC}=25$

24

Å for a (2×2) cell of graphene ($a_{SC}=b_{SC}=9.85$ Å for a (4×4) cell). The distance between the graphene plane and its images (c_{SC}) is large enough to avoid any interactions between them. According to the Monkhorst–Pack scheme, [40] the Brillouin zone was sampled by $(31 \times 31 \times 1)$ and $(15 \times 15 \times 1)$ special mesh points in K space for (2×2) and (4×4) graphene cells, respectively. Full structural optimizations were carried out using the conjugate gradient (CG) algorithm until the maximum residual forces were less than 0.02 eV/Å and the total pressure of the system was smaller than 0.1 kbar per unit cell. The convergence criterion for energy was chosen as 10^{-5} eV between CG steps.

2.3 Results and discussion

We first consider pure graphene coated with Ca atoms, supposing that metal atoms are dispersed uniformly on the surface. As illustrated in Figure 2.1, (2×2) and (4×4) cells of graphene with periodic boundary conditions are considered to compare dense and sparse coverage of Ca on the surface, respectively. In a (2×2) cell (Figure 2.1a), the average Ca–Ca distance is 4.96 Å, which is larger than that of bulk Ca (3.82 Å [25]) but still the Ca atoms have some interactions. However, a large distance of 9.85 Å in a (4×4) cell results in a negligible interaction between Ca atoms. Our calculations show that the denser Ca coverage in a (2×2) cell is energetically more favorable and stable than a (4×4) cell (see E_b values in Figure 2.1a–c) due to Ca's tendency to aggregate. We also investigate different sites of adsorption and find that the H site (namely the hollow site above the center of the hexagon) is the most favorable site for both single and double-sided adsorption. The Ca atom adsorbed on the H site has a binding energy (E_b) of 1.09 and 1.2 eV for single and double-sided coverage, respectively. In the double-sided configuration, the binding energy of the second Ca atom is more than that of single-sided adsorption by 0.11 eV, which is due to the electric field produced by the first Ca atom. Our results are consistent with earlier research on Ca-decorated carbon nanostructures; Yoon et al. [21] found that Ca and Sr bind strongly on top of a hexagonal ring of a C_{60} fullerene with a binding

strength of ~ 1.3 eV, which is roughly half of that of Ti. By DFT computations, Yang et al. [25] showed that the binding energies of Ca adsorbates with the coverage of 50% on the (5,0) and (4,0) nanotubes are 1.62 and 1.94 eV, respectively. They also found that Ca binding energy on the nanotubes with the same chirality decreases as the diameter of the tube increases (e.g. for the (7,0) tube, E_b is 1.32 eV).
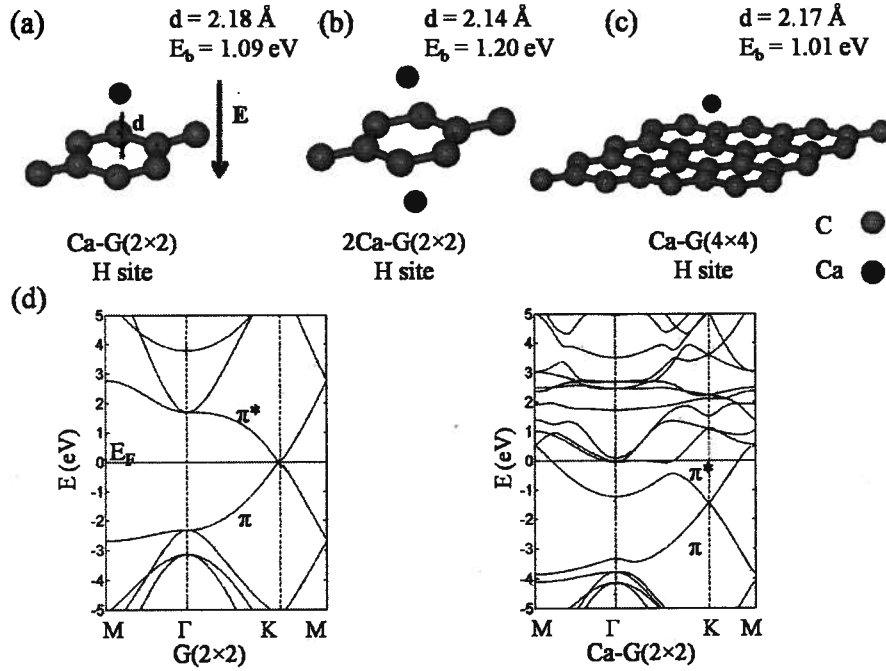
Figure 2.1: (a) The optimized structure of a single Ca atom adsorbed on the H site of the (2×2) cell of graphene (G(2×2)) and the calculated adsorption energy and bond length. (b) Double-sided adsorption of Ca atoms on the H site of graphene. (c) Single-sided adsorption of Ca on a (4×4) cell of graphene (G(4×4)). (d) The calculated energy band structures of bare and Ca-coated graphene folded to the (2×2) cell. It is seen that upon Ca adsorption, the π^* bands of graphene are occupied and distorted. The Fermi energy E_F is set to zero.

Similar to the binding mechanism of Ca on C_{60}, Ca donates its $4s$ electrons to

graphene easily due to its relatively low ionization potential, and the donated electrons partially fill the carbon π^* states. As the Ca atom is brought close to the surface, due to the formation of an electric field between Ca and the graphene plane, C atoms back-donate part of their received electrons to the available empty $3d$ orbitals, resulting in a strong hybridization between the carbon π^* and calcium d states. The resulting charge transfer (i.e. positive charge on the Ca atom), calculated by Mulliken population analysis, is ~ 0.36 and ~ 0.40 electrons for single and double-sided coating, respectively. The calculated band structures of bare and Ca-coated graphene show that carbon's empty π^* bonds in graphene accommodate the transfered charge and accordingly get distorted (Figure 2.1d). The occupied π^* bonds bring up the Fermi energy level and consequently semimetallic graphene becomes metalized.

Then, the double-sided adsorption of hydrogen molecules by the Ca-coated (2×2) cell of graphene with periodic boundary conditions is studied (Figure 2.2). Our calculations show that the resulting electric field between Ca and graphene is strong enough to attract up to 4 H_2 molecules per Ca atom. When we add the fifth H_2 molecule, it cannot make a strong enough bond with the Ca atom. The calculated binding energies of hydrogen molecules on graphene are summarized in Table 2.1 showing both LDA and GGA results, where $E_b = E_{H_2-host}-(E_{H_2}+E_{host})$. Here, all energies are calculated for the corresponding optimized structures. The results show that hydrogen adsorbs on Ca-coated graphene with an average binding energy of ~ 0.43 eV and ~ 0.16 eV per hydrogen according to LDA and GGA, respectively. Overall trends in the GGA calculations are found to be similar to those obtained using LDA while the adsorption energies of H_2 molecules to the Ca atom are about half of the LDA values. These results are in good agreement with Ref[21], where the calculated average H_2 binding energy on CaC_{60} is 0.2 eV/H_2 according to GGA and 0.4 eV/H_2 if LDA is employed. The optimized physical quantities shown in Table 2.1, such as hydrogen binding energy and H-Ca bond length, do not change significantly as the number of H_2 molecules increase, unlike in early transition metal (i.e. Sc, Ti, and V) coatings, where the first hydrogen molecule is dissociated due to

its strong interaction with the TM atom [11, 12]. Such optimal molecular hydrogen binding energies in case of Ca make hydrogen adsorption and desorption feasible at ambient conditions for all of the adsorbed hydrogens. Similar results were obtained by Ataca et al. [24]. Adsorption of four hydrogen molecules on each Ca atom in the (2×2) cell of graphene results in a hydrogen storage capacity of 8.32 wt.%.
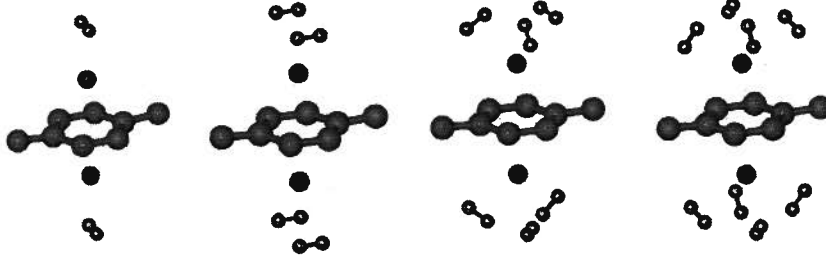
Figure 2.2: Optimized structures of Ca-decorated pure graphene (Ca-G(2×2)) with one to four H_2 molecules, obtained by LDA calculations. In single and double H_2 adsorption, the adsorbed molecules are parallel to graphene. The adsorbed H_2 molecules tend to tilt toward the Ca atom upon adding the third and fourth hydrogen molecules.

	E_b (eV/H_2)		d(H-Ca) (Å)		d(H-H) (Å)	
	LDA	GGA	LDA	GGA	LDA	GGA
$CaG(2 \times 2)H_2$	0.254	0.075	2.29	2.42	0.81	0.83
$CaG(2 \times 2)(H_2)_2$	0.413	0.142	2.28	2.38	0.84	0.82
$CaG(2 \times 2)(H_2)_3$	0.609	0.270	2.21	2.27	0.87	0.84
$CaG(2 \times 2)(H_2)_4$	0.456	0.164	2.22	2.29	0.86	0.83

Table 2.1: Average adsorption energies of hydrogen molecules on Ca-decorated pure graphene and the corresponding bond lengths for one to four adsorbed H_2 molecules per Ca atom. Both LDA (CA) and GGA (PBE) DFT-level calculation results are presented.

In all the above calculations, Ca atoms are assumed to be uniformly distributed

on the graphene plane. However, the calculated adsorption energy of single-sided (double-sided) Ca atoms on (2×2) cell of graphene (with the average Ca-Ca distance of 4.96 Å on one side) is 1.09 eV (1.2 eV) which is smaller than the Ca cohesive energy ($\sim$ 1.8 eV). Thus metal aggregation could actually take place on pure graphene which decreases the storage capacity of system. To have a stable decoration of Ca on graphene, the Ca-graphene adsorption energy should be enhanced to be more than the Ca cohesive energy in bulk Ca.

One way to enhance the metal adsorption strength on graphene plane is to dope graphene with acceptors such as boron atoms. Our calculations show that upon substitutional boron doping the clustering problem can be prevented. As shown in Figure 2.3, the adsorption energy of Ca is enhanced to 2.86, 2.98, and 3.82 eV for single, pair, and triplet B-doped (2×2) cells (with single-sided Ca coating), respectively. These binding energies are much higher than that of Ca's cohesive energy. Corresponding band structures (Figure 2.3) show that in B-doped configurations the π and π^* bands are shifted above the Fermi level as the empty p_z orbital of the boron atom acts as a strong charge accepting center. As a result, the B-doping forms an electron-deficient structure and this deficiency increases as the number of B atoms increases. Charge transfers from Ca atom to graphene occur more efficiently for these electron-deficient structures leading to stronger Ca-graphene binding.

29
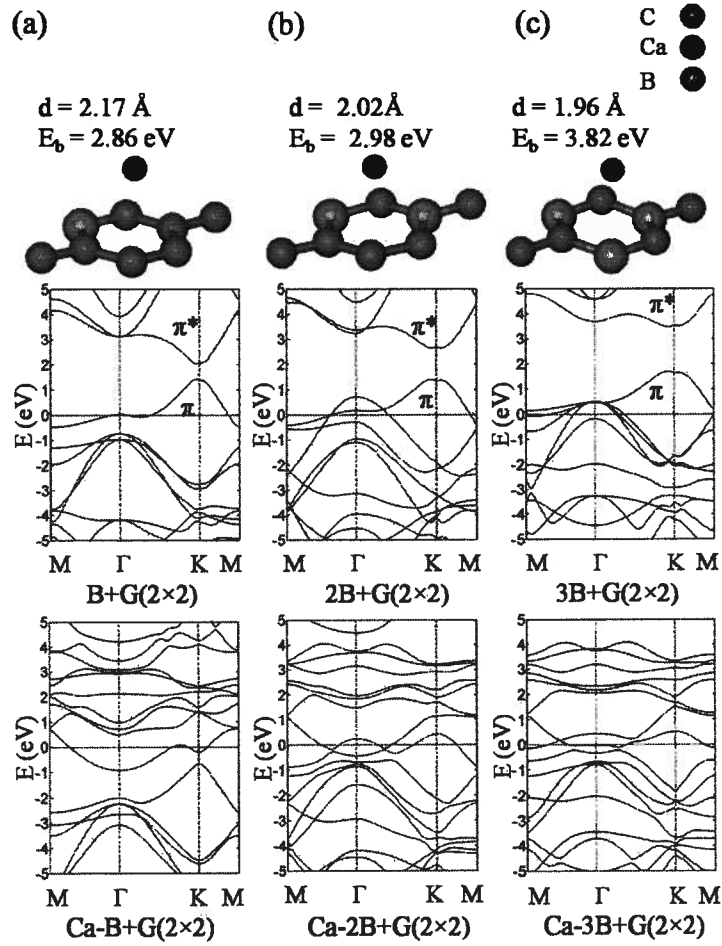
Figure 2.3: The optimized structures, binding energies, bond lengths and energy band diagrams of a single Ca atom adsorbed on the H site of a (2×2) cell with PBC of (a) single B-doped, (b) pair B-doped, and (c) triplet B-doped configurations.

To provide a more explicit analysis of metal stability in B-doped structures, we calculate the binding energy of a Ca dimer and two isolated Ca atoms on pure and B-doped (4×4) cell of graphene (Figure 2.4). These calculations show that the dimerized Ca atom on pure graphene is energetically more favorable by ~ 0.4 eV as compared with the isolated case. In contrast, for the B-doped structure, the

30

energy of the isolated configuration is ∼ 0.2 eV lower than that of the dimerized case. Therefore, Ca can be individually dispersed on a single B-doped graphene. In contrast to calcium, TM atoms (such as Sc,V and Ti) have been found to prefer the dimer form in single and pair B-doped graphene, while they form separated metal atoms in the triplet B-doped configuration [41]. It has been experimentally observed that B doping concentration in graphene can be up to 20 at.% [29, 30]. Thereofore, a triplet B-doped configuration, with the doping concentration of ∼ 38%, may not be a stable structure. Consequently, we can say that solving the clustering problem in Ca-decorated graphene could be more practical than in TM-coated graphene.
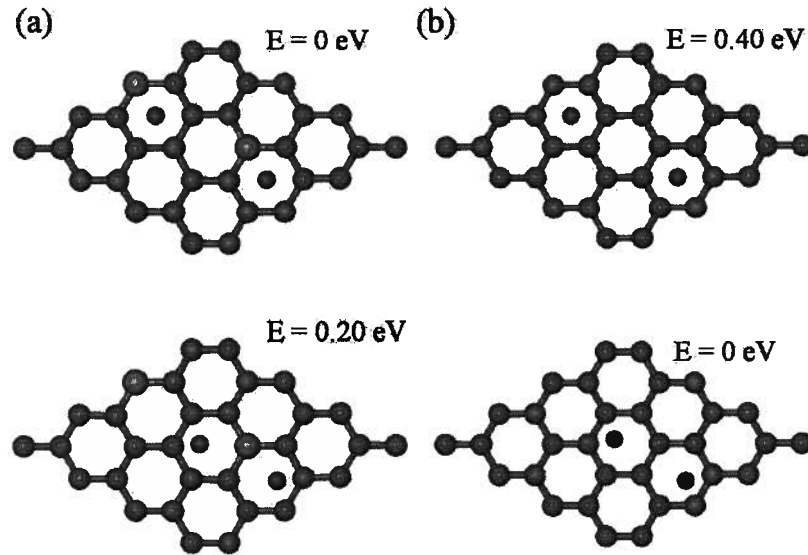
Figure 2.4: Optimized structures of dimerized and separated Ca atoms adsorbed on pure (a) and B-doped (b) (4 × 4) cells of graphene. Our calculations show that in the B-doped structure the isolated configuration is energetically more favorable by ∼ 0.2 eV while in the pure configuration the dimerized configuration is more stable by ∼ 0.4 eV.

Now, we investigate hydrogen adsorption on B-doped structures using LDA calculations. For this study we consider one-sided Ca coating and compare binding energies

of adsorbed H_2 molecules on different boron-doped configurations. Here, the maximum number of adsorbed H_2 per adsorbed Ca atom is still four for the (2×2) coverage similar to that of pure graphene. The average binding energies of the H_2 molecule on single, pair, and triplet structures are ~ 0.42, ~ 0.39, and ~ 0.38 eV/H_2, respectively, which is close to the average E_b of H_2 molecules on pure graphene (~ 0.43 eV/H_2). However, the binding energy of the first H_2 molecule to the Ca atom which prefers to be parallel to the graphene layer is generally decreased by ~ 0.1 eV.

The binding mechanism of H_2 on Ca coated graphene is analogous to that of H_2 on TM coated graphene. Two binding mechanisms contribute to the H_2 adsorption on Ca which are polarization of the H_2 molecule under the electric field produced by the Ca atom and hybridization of the Ca *3d* orbitals with the H_2 σ orbitals [23, 24]. Figure 2.5 displays the projected density of states (PDOS) for the H_2 molecules and Ca *3d* orbitals when one hydrogen molecule is adsorbed on a pure and triplet B-doped graphene. We think that the lower binding energy of the first hydrogen molecule on B-doped graphene can be attributed to less hybridization of H_2 σ and Ca *3d* orbitals below the Fermi level (Figure 2.5).

The above calculations were performed using DFT, and the accuracy of the relatively weak binding energies obtained with this method is questionable. As Table 2.1 shows, binding energies calculated with LDA are more than those of GGA results. To evaluate our DFT calculations, we performed MP2 simulations. MP2 is expected to provide a good description of dispersive interactions, which is missing in DFT calculations. The comparison was carried out with the Gaussian 03 package [42] using the molecular model of coronene (six benzene rings passivated with hydrogen) as a model for a graphene fragment (PBCs are not available for MP2 in Gaussian)(Figure 2.6). This model has previously been shown to provide an adequate representation of graphene for the purpose of binding energy calculations [43]. The structural optimizations and binding energy calculations were performed using double-zeta polarized 6-31G(d,p) and triple-zeta polarized 6-311G(d,p) basis sets, respectively. In our DFT calculations in Gaussian, GGA is described by the PBE functional. Also, LDA is described by the Slater exchange plus Vosko-Wilk-Nusair

correlation (SVWN5) [44] which fits the Ceperely-Alder solution to the uniform electron gas [45]. The results are summarized in Table 2.2. It can be seen that LDA gives almost the same results as MP2 for both energies and strcutures.
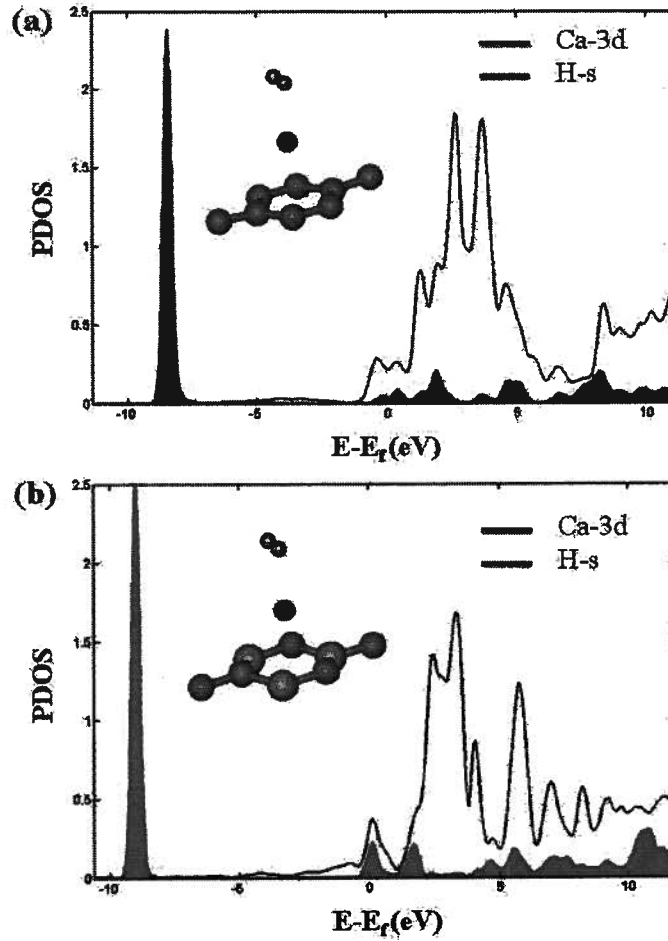
Figure 2.5: Projected density of states (PDOS) of the Ca 3d orbitals and H_2 σ orbitals involved in the adsorption of hydrogen on a (a) Ca-decorated pure graphene and (b) Ca-decorated triplet B-doped graphene. The Fermi energy E_F is set to zero.
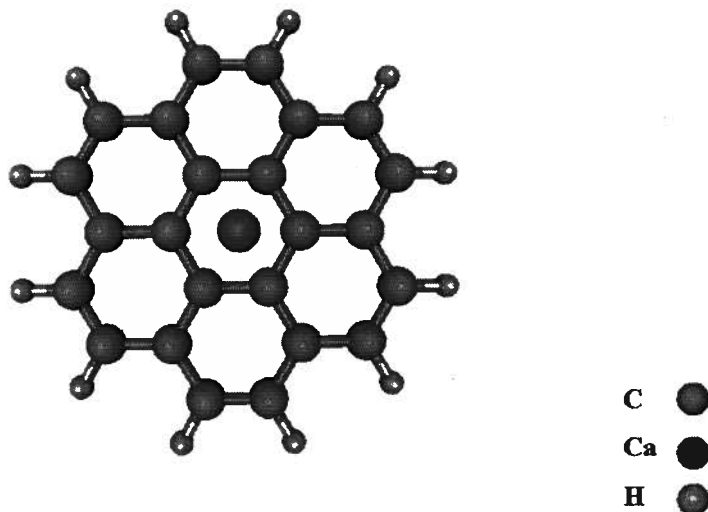
Figure 2.6: Structure of Ca attached to a pure coronene molecule. This molecular model has previously been shown to provide an adequate representation of graphene for the purpose of binding energy calculations.

	d(Ca-C)	d(H-Ca)	d(H-H)	E_b(Ca-C)	E_b(H-Ca)
SVWN5	3.30	4.56	0.77	0.233	0.007
PBE	4.08	6.81	0.75	0.007	0.002
MP2	3.60	5.30	0.73	0.382	0.005

Table 2.2: Comparison of binding energies (in eV) and bond lengths (in Å) obtained by LDA (SVWN5), GGA (PBE), and MP2 calculations on the molecular model of Coronene.

2.4 Conclusion

In conclusion, we have studied the metal dispersion and hydrogen binding properties on Ca-coated B-doped graphene. It is found that a stable decoration of Ca atoms on graphene can be obtained upon substitutional boron doping. Our calculations show that individual calcium atoms are stable on a single B-doped (2×2) cell of graphene (i.e. with a concentration of 12 at.% boron doping). The double-sided Ca-decorated single B-doped graphene can reach a gravimetric capacity of 8.38 wt.%. We encourage an experimental research to synthesize these hydrogen storage nanomaterials that may operate at room temperature and ambient pressure.

Bibliography

[1] Schlapbach, L.; Züttel, A. *Nature (London)* **2001**, *414*, 353–358.

[2] Bhatia, S. K.; Myers, A. L. *Langmuir* **2006**, *22*, 1688–1700.

[3] Lochan, R. C.; Head-Gordon, M. *Phys. Chem. Chem. Phys.* **2006**, *8*, 1357–1370.

[4] Dillon, A. C.; Jones, K. M.; Bekkedahl, T. A.; Kiang, C. H.; Bethune, D. S.; Heben, M. J. *Nature* **1997**, *386*, 377–379.

[5] Chambers, A.; Park, C.; Baker, R. T. K.; Rodriguez, N. M. *J. Phys. Chem. B* **1998**, *102*, 4253–4256.

[6] Liu, C.; Fan, Y. Y.; Liu, M.; Cong, H. T.; Cheng, H. M.; Dresselhaus, M. S. *Science* **1999**, *286*, 1127–1129.

[7] Ritschel, M.; Uhlemann, M.; Gutfleisch, O.; Leonhardt, A.; Graff, A.; Täschner, C.; Fink, J. *Appl. Phys. Lett.* **2002**, *80*, 2985–2987.

[8] Hirscher, M.; Becher, M.; Haluska, M.; Quintel, A.; Skakalova, V.; Choi, Y. M.; Dettlaff-Weglikowska, U.; Roth, S.; Stepanek, I.; Bernier, P.; Leonhardt, A.; Fink, J. *J Alloys and Compd* **2002**, *330-332*, 654–658.

[9] Panella, B.; Hirscher, M.; Roth, S. *Carbon* **2005**, *43*, 2209–2214.

[10] Zhang, Y.; Franklin, N. W.; Chen, R. J.; Dai, H. *Chem. Phys. Lett.* **2000**, *331*, 35–41.

[11] Yildirim, T.; Ciraci, S. *Phys. Rev. Lett.* **2005**, *94*, 175501.

[12] Zhao, Y.; Kim, Y.; Dillon, A. C.; Heben, M. J.; Zhang, S. B. *Phys. Rev. Lett.* **2005**, *94*, 155504.

[13] Durgun, E.; Ciraci, S.; Yildirim, T. *Phys. Rev. B* **2008**, *77*, 085405.

[14] Mingos, D. M. P. *J. Organomet. Chem.* **2001**, *635*, 1–8.

[15] Kubas, G. J. *Acc. Chem. Res.* **1988**, *21*, 120–128.

[16] Sun, Q.; Wang, Q.; Jena, P.; Kawazoe, Y. *J. Am. Chem. Soc.* **2005**, *127*, 14582.

[17] Durgun, E.; Ciraci, S.; Zhou, W.; Yildirim, T. *Phys. Rev. Lett.* **2006**, *97*, 226102.

[18] Chen, P.; Wu, X.; Lin, J.; Tan, K. L. *Science* **1999**, *285*, 91–93.

[19] Yang, R. T. *Carbon* **2000**, *38*, 623–641.

[20] Dag, S.; Ozturk, Y.; Ciraci, S.; Yildirim, T. *Phys. Rev. B* **2005**, *72*, 155404.

[21] Yoon, M.; Yang, S.; Hicke, C.; Wang, E.; Geohegan, D.; Zhang, Z. *Phys. Rev. Lett.* **2008**, *100*, 206806.

[22] Li, M.; Li, Y.; Zhou, Z.; Shen, P.; Chen, Z. *Nano Lett.* **2009**, *9*, 1944–1948.

[23] Lee, H.; Ihm, J.; Cohen, M. L.; Louie, S. G. *Phys. Rev. B* **2009**, *80*, 115412.

[24] Ataca, C.; Aktürk, E.; Ciraci, S. *Phys. Rev. B* **2009**, *79*, 041406.

[25] Yang, X.; Zhang, R. Q.; Ni, J. *Phys. Rev. B* **2009**, *79*, 075431.

[26] Sun, Y. Y.; Lee, K.; Kim, Y.; Zhang, S. B. *Appl. Phys. Lett.* **2009**, *95*, 033109.

[27] Novoselov, K. S.; Geim, A. K.; Morozov, S. V.; Jiang, D.; Zhang, Y.; Dubonos, S. V.; Grigorieva, I. V.; Firsov, A. A. *Science* **2004**, *306*, 666–669.

[28] Züttel, A.; Sudan, P.; Mauron, P.; Kiyobayashi, T.; Emmenegger, C.; Schlapbach, L. *Int. J. Hydrogen Energy* **2002**, *27*, 203–212.

[29] Way, B. M.; Dahn, J. R.; Tiedje, T.; Myrtle, K.; Kasrai, M. *Phys. Rev. B* **1992**, *46*, 1697.

[30] Shirasaki, T.; Derré, A.; Ménétrier, M.; Tressaud, A.; Flandrois, S. *Carbon* **2000**, *38*, 1461–1467.

[31] Soler, J. M.; Artacho, E.; Gale, J. D.; García, A.; Junquera, J.; Ordejón, P.; Sánchez-Portal, D. *J. Phys.: Condens. Matter* **2002**, *14*, 2745–2779.

[32] Kleinman, L.; Bylander, D. M. *Phys. Rev. Lett.* **1982**, *48*, 1425–1428.

[33] Troullier, N.; Martins, J. L. *Phys. Rev. B* **1991**, *43*, 1993–2006.

[34] Perdew, J. P.; Zunger, A. *Phys. Rev. B* **1981**, *23*, 5048–5079.

[35] Perdew, J. P.; Burke, K.; Ernzerhof, M. *Phys. Rev. Lett.* **1996**, *77*, 3865–3868.

[36] Okamoto, Y.; Miyamoto, Y. *J. Phys. Chem. B* **2001**, *105*, 3470–3474.

[37] Moller, C.; Plesset, M. S. *Phys. Rev.* **1934**, *46*, 618–622.

[38] Louie, S. G.; Froyen, S.; Cohen, M. L. *Phys. Rev. B* **1982**, *26*, 1738–1742.

[39] Machón, M.; Reich, S.; Thomsen, C.; Sánchez-Portal, D.; Ordejón, P. *Phys. Rev. B* **2002**, *66*, 155410.

[40] Monkhorst, H. J.; Pack, J. D. *Phys. Rev. B* **1976**, *13*, 5188–5191.

[41] Kim, G.; Jhi, S. *Phys. Rev. B* **2008**, *78*, 085408.

[42] Frisch, M. J. et al. *Gaussian 03, Revision C.02*, Gaussian, Inc., Wallingford, CT, 2004.

[43] Heine, T.; Zhechkov, L.; Seifert, G. *Phys. Chem. Chem. Phys.* **2004**, *6*, 980–984.

[44] Vosko, S. H.; Wilk, L.; Nusair, M. *Can. J. Phys.* **1980**, *58*, 1200.

[45] Ceperley, D. M.; Alder, B. J. *Phys. Rev. Lett.* **1980**, *45*, 566–569.

Chapter 3

Summary, Conclusions and Future Work

Hydrogen has been recognized as a highly appealing energy carrier for renewable energy because of its abundance and environmental friendliness. To achieve economic feasibility, hydrogen storage materials with high gravimetric and volumetric densities must be developed. Furthermore, hydrogen recycling should be performed reversibly under near ambient conditions. The current state of the art is at an impasse in providing a storage material that meets a storage capacity of 9 wt.% or more. In recent years, carbon nanomaterials have been widely studied for their application in hydrogen storage [1, 2, 3, 4]. However, pristine carbon nanostructures are chemically too inert to be useful for practical hydrogen storage [5, 6].

Recently, transition metal-decorated carbon nanostructures have been proposed to satisfy the above requirements [7, 8]. The metal-hydrogen binding energy and ratio look very promising with respect to the capacity and release temperature. However, the issues of structural stability and poor reversibility in transition metal (TM) dispersions are major concerns in developing a practical storage material [9]. In 2008, for the first time, Yoon et al. [10] suggested calcium-coated C_{60} fullerenes for high capacity hydrogen storage.

As discussed in Chapter 2, we explored theoretically hydrogen adsorption and storage in calcium-decorated boron-doped graphene. Our results were carried out using density functional theory (DFT) and the SIESTA simulation package. First, we

considered the pristine graphene plane functionalized by calcium coating. Calcium atoms were assumed to be uniformly distributed on both sides of graphene with a coverage of 25%. Calcium strongly binds to graphene due to the charge transfer between Ca and the graphene plane. We found that a (2×2) cell of graphene (with periodic boundary conditions) coated with 2 Ca atoms on both sides, can store up to eight hydrogen molecules with an average binding energy of ~ 0.4 eV/H_2. In this case, the corresponding gravimetric density is 8.32 wt.% hydrogen.

In Chapter 2, we also addressed the important issue of metal clustering. Our energy calculations show that calcium atoms tend to form clusters on pristine graphene because of the small binding energy of Ca to graphene. Consequently, the hydrogen storage capacity is decreased due to metal aggregation. One possible way to have a stable decoration of Ca atoms on graphene is to dope the substrate with boron atoms. A boron atom acts as a strong charge accepting center and consequently the clustering could be prevented in B-doped configurations. Our calculations show that individual calcium atoms are stable on a single B-doped (2×2) cell of graphene (i.e. with a concentration of 12 at.% boron doping). The double-sided Ca-decorated single B-doped graphene can reach a gravimetric capacity of 8.38 wt.%.

Our results advance our fundamental understanding of adsorption of hydrogen in calcium-decorated graphene and suggest new routes to better storage systems. Obviously, investigating the effect of different parameters in our calculations is an immediate further work that can easily be performed. In the first instance, we could explore the effect of distance between graphene planes. Here, we chose a large distance of 25 Å between graphene and its periodic images to ensure negligible interaction between neighboring planes. In future work, we can study the effect of the interaction between two graphene planes on hydrogen adsorption and storage. Moreover, we could investigate energy variations and reaction paths for molecular adsorption and desorption of hydrogen on a Ca-decorated graphene to have a better understanding of our storage system. We hope that these theoretical studies motivate an active line of experimental efforts towards novel materials needed for hydrogen storage in the fuel cell technology.

Bibliography

[1] Dillon, A. C.; Jones, K. M.; Bekkedahl, T. A.; Kiang, C. H.; Bethune, D. S.; Heben, M. J. *Nature* **1997**, *386*, 377–379.

[2] Züttel, A.; Sudan, P.; Mauron, P.; Kiyobayashi, T.; Emmenegger, C.; Schlapbach, L. *Int. J. Hydrogen Energy* **2002**, *27*, 203–212.

[3] Ritschel, M.; Uhlemann, M.; Gutfleisch, O.; Leonhardt, A.; Graff, A.; Täschner, C.; Fink, J. *Appl. Phys. Lett.* **2002**, *80*, 2985–2987.

[4] Chambers, A.; Park, C.; Baker, R. T. K.; Rodriguez, N. M. *J. Phys. Chem. B* **1998**, *102*, 4253–4256.

[5] Brown, C.; Yildirim, T.; Neumann, D.; Heben, M.; Dillon, T. G. A.; Alleman, J.; Fischer, J. *Chem. Phys. Lett.* **2000**, *329*, 311–316.

[6] Dag, S.; Ozturk, Y.; Ciraci, S.; Yildirim, T. *Phys. Rev. B* **2005**, *72*, 155404.

[7] Zhao, Y.; Kim, Y.; Dillon, A. C.; Heben, M. J.; Zhang, S. B. *Phys. Rev. Lett.* **2005**, *94*, 155504.

[8] Yildirim, T.; Ciraci, S. *Phys. Rev. Lett.* **2005**, *94*, 175501.

[9] Zhang, Y.; Franklin, N. W.; Chen, R. J.; Dai, H. *Chem. Phys. Lett.* **2000**, *331*, 35–41.

[10] Yoon, M.; Yang, S.; Hicke, C.; Wang, E.; Geohegan, D.; Zhang, Z. *Phys. Rev. Lett.* **2008**, *100*, 206806.